JOURNAL OF MATERIALS SCIENCE 22 (1987) 2051–2057

Lifetime predictions for a ceramic cutting tool material at high temperatures

B. GURUMOORTHY
Department of Mechanical Engineering, Carnegie Mellon University, Pittsburgh, Pennsylvania 15213, USA

K. KROMP
Institut für Werkstoffwiss, Max-Planck Institut für Metallforschung, Stuttgart, West Germany

F. B. PRINZ
Department of Mechanical Engineering, Carnegie Mellon University, Pittsburgh, Pennsylvania 15213, USA

A. C. BORNHAUSER
Technische Universität, Institut für Nichtmetallische Werkstoffe, Berlin, West Germany

Dynamic loading experiments are performed at different loading rates and temperatures in three-point bending with a commercial cutting tool material. Strength data from time-dependent failure analysis are combined with Weibull statistics to make lifetime predictions for static loading (STP diagrams). Stress corrosion is concluded to be active from ambient temperatures up to 1100° C. Additionally at high temperatures an energy dissipation process caused by plastic and viscous second phase is activated. Both these mechanisms are interacting. With the application of Weibull statistics, strength data are shown to be strongly influenced by the area of loaded surface.

1. Introduction

The development of ceramic components for any application involves the correlation of the material properties and the material requirements, as defined by the in-service conditions (stress, temperature levels). Much of the required information about the material capability can be presented on a strength–time–probability (STP) diagram [1, 2]. For given conditions of temperature and stress this diagram enables the design of a component for specific lifetimes and survival probabilities. The development of the STP diagrams is based on the existence of models to estimate the lifetime of ceramic material under stress, from data on the stress-rate dependence of strength.

For these design diagrams to be of any use in the design of a component, the data on dynamic fatigue have to be available for relevant conditions of temperature and environment. Most of the work with regard to establishing the STP diagrams, however, has been done at room temperature [2, 3]. Ceramics are increasingly finding use in high-temperature applications like metal cutting and as engine components. There is a need, therefore, to obtain data on the variation of strength with stress rate and establish the STP diagrams, at these high temperatures. If the models for lifetime prediction that are valid at room temperature and not valid at the higher temperatures, the mechanism of crack growth at those temperatures has to be understood to enable the development of models to predict the lifetimes of ceramic material.

2. Strength–probability–time relationships in ceramics

The strength of ceramic materials is controlled by the stress required to propagate small microstructural flaws. Variation in strength is thus inherent due to the range of flaw sizes. In the case of ceramic materials there occurs a degradation in the strength of the material with time. Information is thus required on

(i) the statistical variation in strength,
(ii) the variation of strength with time, and
(iii) the combination of statistics and strength variation with time under relevant conditions of temperature and environment.

2.1. Statistical variations in strength

In the measurement of the fracture strength of a brittle material, essentially one or several of the large flaws are caused to propagate. The statistics of fracture strength hence relate to the extreme-value distribution function. One such statistical function due to Weibull [4] has found wide application in describing the strength variation of ceramics. Weibull's function is based on a weakest-link model. He proposed that a body, volume V, contains a statistical distribution of non-interacting inhomogeneities. Fracture then occurs when any one inhomogeneity reaches critical severity in this volume. The probability of failure then relates to the probability of occurrence of the critical inhomogeneity in the volume V and is given by

0022–2461/87 $03.00 + .12

$$P_f = 1 - \exp\left[-\frac{V}{V_0}\left(\frac{\sigma_f - \sigma_u}{\sigma_0}\right)^m\right] \quad (1)$$

where σ_f is the fracture stress and σ_u is the stress below which fracture is assumed to have zero probability (this stress is mostly taken to be zero). σ_0 and V_0 are normalizing parameters; m is a number and is known as the Weibull modulus. It reflects the degree of variability in the strength of the material – the greater the value of m is, the less variable is the strength. For ceramics m varies typically between 5 and 20. Any extrapolation based on the distribution given by Equation 1 is valid only if the material and the mechanism of failure remain the same. The distribution given by Equation 1 can be used to account for effects of changes in geometry and loading.

When σ_u can be taken to be zero and no information is available for σ_0 and V_0, the "standardized Weibull distribution" [5] is used:

$$P_f = 1 - \exp\left[-\left(\frac{S}{S_0}\right)^m\right] \quad (2)$$

S is the fracture stress and S_0 is a normalizing parameter. This function describes the experimental results sufficiently, but lacks any physical basis.

2.2. Time dependence of strength

Time-dependent degradation of strength of the ceramic material occurs due to subcritical crack growth. A stress-dependent chemical interaction between the material and its environment has been identified as the cause of this phenomenon [6]. The time-dependent failure characteristics can be predicted empirically by the stress intensity (K_I) and crack velocity ($v = \dot{a}$) data. A typical K_I against v plot is shown in Fig. 1. There are three regions. In Region I the rate of chemical reaction at the crack front controls the crack growth, described by the experimentally proved empirical equation

$$v = AK_I^n \quad (3)$$

In Region II the diffusion and/or flux of the corrosive species to the crack front controls the growth. The Region III shown in Fig. 1 is independent of the corrosive species and describes crack growth by thermal activation, important only at high temperatures. In the presence of a corrosive environment Region II is also negligible for alumina.

If the crack growth rate is described by Equation 3,

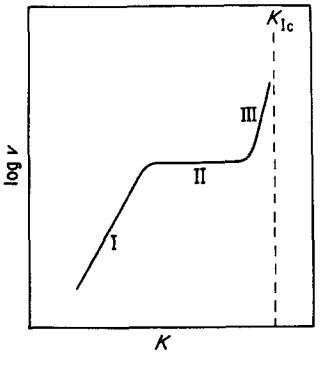

Figure 1 Stress intensity K_I against crack velocity diagram, schematic.

then from this relation and the relation between the stress intensity K_I, flaw size a and the applied stress σ given by

$$K_I = \sigma Y a^{1/2} \quad (4)$$

where Y is a dimensionless geometric factor, related to specimen dimension, the failure time t_{fs} for static loading can be obtained as

$$t_{fs} = \frac{B}{S_{fs}^n} \quad (5)$$

with

$$B = \frac{2a_c^{(2-n)/2}}{Y^2 A(n-2)}$$

where S_{fs} is the applied static load and a_c is the initial critical defect length.

2.3. SPT and STP diagrams

The stress–probability–time (SPT) diagram can be derived by combining the statistical distribution of Equation 2 and the time-dependent failure analysis as described in the previous section [2, 7, 8]. The basic assumption is that the statistical distribution for static loading is related to that for dynamic loading. It is assumed that the same fracture stress values S_{fs}, S_{fd} respectively, can be obtained in both static and in dynamic loading. The failure time under static load, t_{fs}, and the failure time under dynamic load, t_{fd}, are related by [2]

$$t_{fs} = \frac{1}{n+1} t_{fd} \quad (6)$$

The distribution for dynamic loading can be related to a normalized distribution for static loading. Hence the static lifetime t_{fs} as calculated by Equation 6 can be transformed to the corresponding normalized static lifetime t_N.

$$\frac{t_{fs}}{t_N} = \left(\frac{S_N}{S_{fd}}\right)^n \quad \text{for } S_{fd} = S_{fs} \quad (7)$$

Furthermore, the normalized strength S_N can be written (from Equations 6 and 7) as

$$S_N = \left(\frac{S_{fd}}{(n+1)\dot{S}t_N}\right)^{1/n} S_{fd} \quad (8)$$

with $S_{fd} = \dot{S}t_{fd}$. Replacing the value S_{fd} from Equation 8 in Equation 2,

$$P_{fN} = 1 - \exp\left[\left(\frac{S_N}{S_{ON}}\right)^{m_N}\right] \quad (9)$$

where

$$S_{ON} = \left(\frac{S_0}{(n+1)\dot{S}t_N}\right)^{1/n} S_0 \quad \text{and} \quad m_N = \frac{mn}{n+1}$$

Equation 9 gives the distribution of the normalized strength values and forms the basis for the SPT and STP diagrams.

This equation can be used to generate SPT and STP plots once the values of n and the Weibull parameters m and S_0 for the dynamic measurements are determined. The SPT diagram is a plot of the probability of

TABLE I Specimen composition (material sintered at 1600° C)

Zirconium oxide in non-transform state	12 wt %
Tungsten carbide	2 wt %
Cobalt	< 0.2 wt %
Aluminium oxide	balance

failure against stress for various lifetimes, and the STP diagram is a plot of lifetime against stress for various probabilities of failure.

3. Experimental methods

Experiments were conducted to measure the stress-rate dependence of the fracture strength (S) at various temperatures. Specimens were fractured in a three-point bending device at two or three different stress rates. The stress rates differed by two orders of magnitude.

The specimens were made of a commercial cutting-tool material. The composition can be seen in Table I. The experiments were carried out using two different experimental devices. The first set of experiments were done in a resistance furnace, enclosed in a vacuum chamber. The high thermal inertia of this furnace resulted in relatively long holding times of approximately 30 min (heating up excluded). Measurements at 22, 350 and 700° C in air and at 700 and 900° C in a vacuum were carried out with this equipment. The stress rates with this equipment were ~ 1.5 and ~ 150 MPa sec^{-1} (Test Series 1). The nominal dimensions of the specimen were 3 mm × 7.2 mm × 35 mm with a span of 28 mm. In this series the specimens were loaded in a flat configuration. i.e. specimen height was 3 mm.

The second device had an induction heating system. With the fast response of the equipment the holding times (including heating up) could be held constant at 10 min for all temperatures and loading rates. Measurements at 700, 900 and 1100° C were carried out with this equipment. The stress rates in this case were ~ 1, ~ 100 and $\sim 10\,000$ MPa sec^{-1}. The specimen dimensions in this case were 3.2 mm × 6 mm × 35 mm and the span was 24 mm. The specimens, in this series, were loaded in an upright position (specimen height = 6 mm).

4. Results

The strength values, S_{fd}, measured in both the test series, were ranked and the corresponding failure probability P_f was calculated as

$$P_f = \frac{i}{N + 1} \tag{10}$$

where i is the rank of the strength value and N the total number of the strength values. The strength values S_{fd} and the associated failure probability P_f were fitted to a normalized Weibull distribution by a linear regression of $\ln \ln [1/(1 - P_f)]$ on $\ln S_{fd}$. The Weibull parameters m and S_0 obtained from the slope and the intercept of the linear fit, respectively, are given in Table II together with the mean values of strength $\bar{S}_{fd}$ for each temperature and stress rate.

The Weibull plots for the strength data at each temperature for the stress rate of 100 MPa sec^{-1} are given in Fig. 2 (plots for 900 and 1100° C are calculated from Test Series 2). From Fig. 2 it is obvious that the Weibull modulus m increases with increasing temperature (compare Table II). The variation in the strength is, therefore, lower at higher temperatures.

At each temperature a linear least-squares analysis was done with $\ln \bar{S}_{fd}$ and $\ln \dot{S}$ ("mean value plot") to obtain the subcritical crack growth exponent n [9–11] (see Table III).

Finally, STP design diagrams were calculated from Equation 9 using the appropriate Weibull parameters m, S_0 and the subcritical crack growth exponent n. Fig. 3 depicts the STP lines that show the lifetime that can be expected at various stress levels for a failure probability of 0.1% (lines for 900 and 1100° C calculated from Test Series 2).

A remarkable difference in the mean values of strength ($\bar{S}_{fd}$, Table II) is observed between the results of test series 1 and 2 at 700° C (the temperature at which the measurements in the two sets of experiments overlap). This difference will be discussed in the next section.

5. Discussion

Table III shows the variation of the subcritical crack growth exponent n with temperature and environment.

TABLE II Mean fracture strengths and Weibull statistics data at different temperatures

T (° C)	Test Series	$\dot{S}$ (MPa sec^{-1})	N	$\bar{S}_{fd}$ (MPa) in air	m	S_0 (MPa)	Correlation coefficient
22	1	1.7	20	604 ± 123	3.5	680	0.881
22	1	166.5	20	646 ± 134	4.8	704	0.990
350	1	1.4	20	406 ± 76	5.3	440	0.972
350	1	136.4	20	487 ± 92	5.4	526	0.997
700	1	0.9	20	344 ± 65	4.0	383	0.862
700	1	100.1	20	397 ± 70	5.7	428	0.988
700	2	2	13	462 ± 71	6.5	493	0.991
700	2	100	13	550 ± 59	9.8	576	0.966
700	2	10 000	13	572 ± 97	6.1	613	0.983
900	2	1	13	231 ± 20	12.5	240	0.948
900	2	100	13	238 ± 25	9.9	250	0.989
900	2	10 000	13	275 ± 22	13.3	285	0.986
1100	2	1	13	166 ± 28	6.4	178	0.977
1100	2	100	13	197 ± 32	6.0	211	0.966
1100	2	10 000	13	218 ± 27	8.3	230	0.990

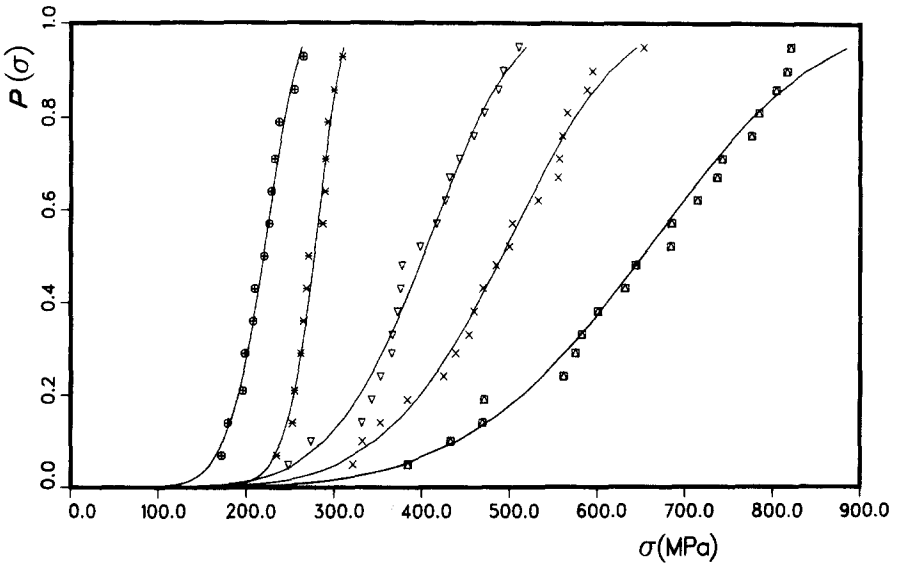

Figure 2 Weibull plots for all measured temperatures, at a loading rate of 100 MPa sec^{-1}; (⊕) 20, (*) 350, (▽) 700, (x) 900 and (⊠) 1100° C.

In air, the increase in temperature affects the subcritical crack growth in two ways:

(a) The partial pressure of the water vapour drops, thereby reducing the corrosive effect.

(b) The higher temperature causes the chemical reactions at the crack tip to occur faster, so that stress corrosion is enhanced.

Up to 700° C the second effect is dominant, since stress corrosion at the crack tip occurs to a larger extent resulting in lower values of n. Once the effect of a lower partial pressure becomes dominant, the value of n increases again with decreasing corrosive influence (Table III).

Negative values of n are obtained in a vacuum (absence of a corrosive medium) at 700 and 900° C, though for a vacuum the n values are expected to be infinite. The negative values of n in a vacuum can be attributed to energy dissipation mechanisms at the crack front.

Thus at high temperature two kinds of mechanisms are active in this material:

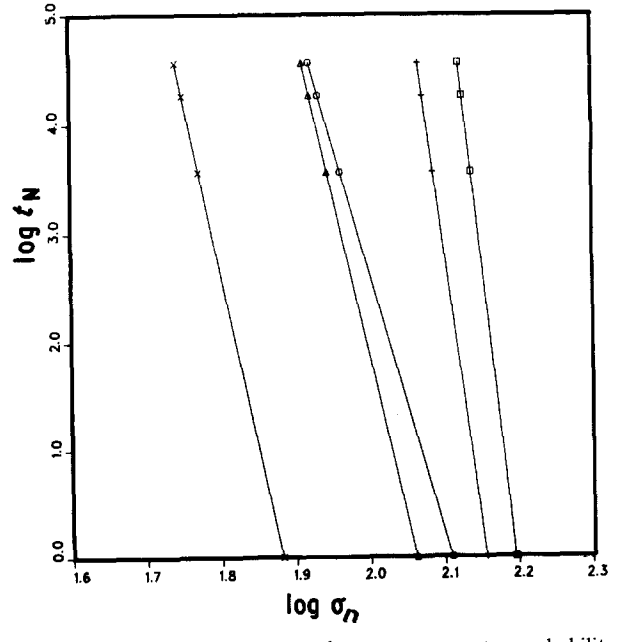

Figure 3 STP lines for all measured temperatures, at a probability of failure 0.1%, σ (MPa), t_N (sec): (□) 20, (+) 350, (○) 700, (△) 900 and (×) 1100° C.

(i) subcritical crack growth by corrosion, and

(ii) an energy dissipation process caused by plastic flow of viscoelastic second phases.

In air the stress corrosion mechanism dominates, with the result that subcritical crack growth occurs, as indicated by positive values of n. In a vacuum stress corrosion is absent, therefore the energy dissipation processes are dominant. With increasing temperature, the energy dissipation increases resulting in the greater negative value for n at 900° C (Table III).

Examination of the fractured surfaces using SEM points to plastic flow of the second phase in the material to be the cause of the energy dissipation. As can be seen from the fractured surfaces at the slowest loading rate of 1 MPa sec^{-1} in air at 700, 900 and 1100° C (Figs 4a, b and c, respectively), the coating of the grains by the second phase is much greater at 1100° C (Fig. 4c) as compared to that at 700° C.

The increase in the value of n as the temperature increases from 700 to 900° C is influenced by both the decreasing corrosive influence of water vapour discussed above and the increasing energy dissipation by the plastic flow of the second phase.

An SEM investigation of the fracture surface of all the specimens broken at 700° C in both the test series (Figs 5 and 6) showed that in most of the specimens, the crack started from the surface (or the edges). This is in violation of the assumption made in arriving at the Weibull function, that the cracks start from the volume of the specimens. Therefore it was

TABLE III Variation of n with temperature and environment

T (° C)	Test Series	n
Air		
22	1	67
350	1	24
700	1	32
700	2	39 ± 17
900	2	52 ± 20
1100	2	33 ± 5
Vacuum		
700	1	−16
900	1	−128

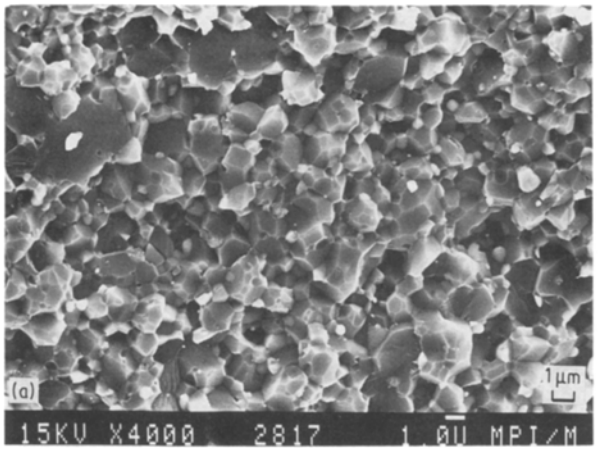

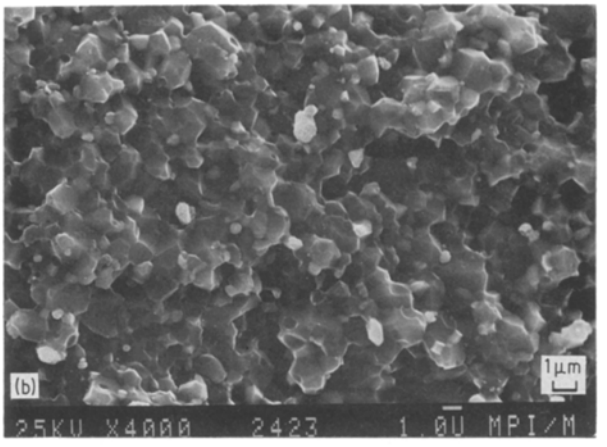

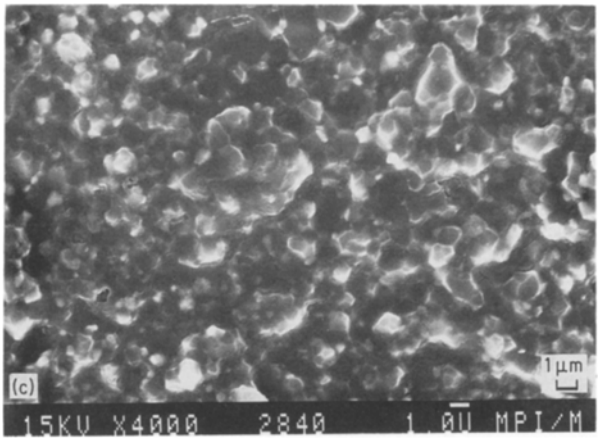

Figure 4 Fracture surface appearance for Test Series 2 at a loading rate of ~ 1 MPa sec^{-1}: (a) 700, (b) 900, (c) 1100° C.

hypothesized that the difference in the strength values between the two test series at 700° C is due to the difference between the loaded surface area in Test Series 1 (specimen held flat) and Test Series 2 (specimen held upright).

The appropriate Weibull function for surface dependence of the crack growth (only the lower surface needs to be considered here) is given by [1, 12]

$$P_f = 1 - \exp\left[-\frac{A}{A_0}\left(\frac{\sigma_f}{\sigma_0}\right)^m \frac{1}{m+1}\right] \quad (11)$$

To prove this hypothesis of surface dependence, first the specimens which had cracked from the volume were separated. New standardized distributions were calculated with the remaining specimens and the corresponding mean values of strength and the Weibull parameters S_0 and m are given in Table IV. Again, the difference in the mean values of strength between the two test series can be observed. Equating the standardized Weibull function (Equation 2) calculated for the reduced set of specimens and the Weibull function for surface dependency (Equation 11), the following relation is obtained:

$$\frac{1}{S_0} = \frac{1}{\sigma_0}\left(\frac{A/A_0}{m+1}\right)^{1/m} \quad (12)$$

Writing Equation 12 for both test series, and noting that σ_0 and A_0 are constants and $A_0^{1/m_2}/A_0^{1/m_1} \sim 1$, the ratio S_{0_2}/S_{0_1} is given by

$$S_{0_2}/S_{0_1} = [(m_2+1)/A_2]^{1/m_2}/[(m_1+1)/A_1]^{1/m_1} \quad (13)$$

Equation 13 thus provides a way to account for the difference in the area of the loaded surface and as can

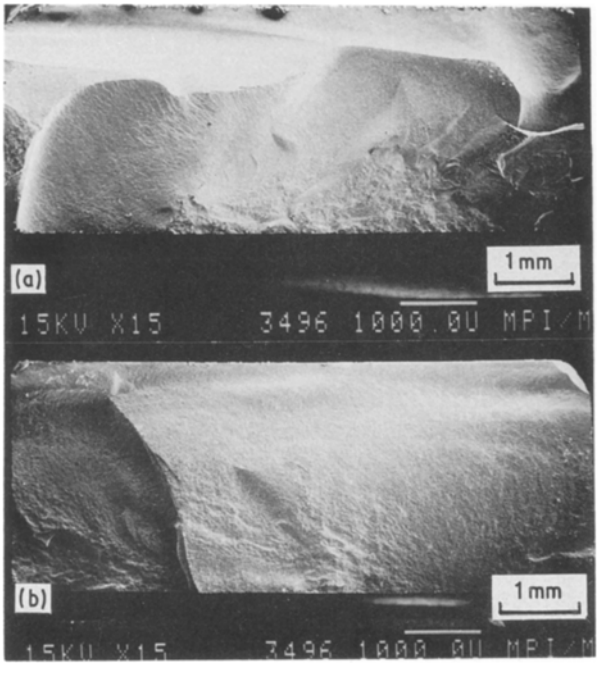

Figure 5 Fracture surface appearance, Test Series 1 (flat loading) at 700° C, loading rate 100 MPa sec^{-1}: (a) crack starting from volume, (b) crack starting from surface.

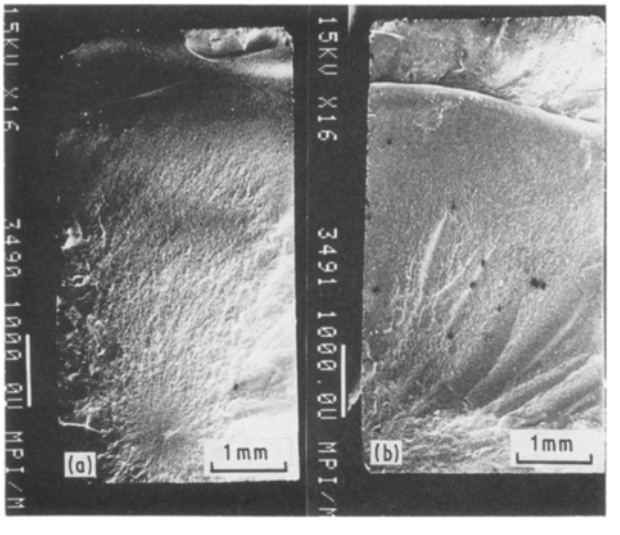

Figure 6 Fracture surface appearance, Test Series 2 (upright loading) at 700° C, loading rate 100 MPa sec^{-1}: (a) crack starting from volume, (b) crack starting from surface.

TABLE IV Mean fracture strengths and Weibull statistics data, loaded areas and coefficients in the Weibull exponents for reduced Weibull functions at 700° C

Test Series	$\dot{S}$ (MPa sec^{-1})	N	$\bar{S}_{fd}$ (MPa)	m	S_0 (MPa)	Correlation coefficient	A (mm^2)	$\left(\frac{m+1}{A}\right)^{1/m}$
1	0.9	12	340 ± 68	4.67	368	0.830	201.6	0.466
2	2	8	452 ± 78	5.56	486	0.973	76.8	0.642
1	100.1	13	411 ± 71	5.95	441	0.973	201.6	0.568
2	100	6	558 ± 43	12.3	578	0.918	76.8	0.867

be seen from Table V, though the distributions are obtained from a small number of specimens, the agreement of the measured parameters with the above relation is obvious.

Therefore, the difference in strength values between the two test series at 700° C is caused by the difference in the loaded areas, which was a consequence of the difference in the loading configuration in the two test series.

6. Concluding remarks

It is clear that at some temperature the stress corrosion mechanism will cease to be active, as the environment responsible for corrosion would have dispersed. Various mechanisms have been proposed to describe the subcritical crack growth mechanism, based on diffusional theories [13, 14] and plastic flow theories [15–17]. While quantitative models exist for these mechanisms, they are not of much use in establishing the design diagrams. This is because they involve too many material parameters. As the failure time is very sensitive to stress, all theories seem to fit the data and it is not possible to distinguish between the various models based on their agreement with the data in the literature [18].

While a comprehensive model to describe the subcritical crack growth mechanism at high temperatures seems far away, empirical models can be developed to make lifetime predictions at these temperatures. The problems due to non-linearity of the load–displacement relation can be eliminated by using a different parameter to describe the relationship between the load and the crack velocity. Two such parameters have been proposed in the literature. The J-integral based on the energy concept [19] is applicable to subcritical crack growth due to elastoplastic reactions. At very low loading rates, however, in addition to the crack growth due to viscous (elastoplastic) reactions, crack growth due to creep also occurs. In such cases the power integral C^* [20] may be a suitable parameter. For the material under investigation the J-integral would be best suited to describe the relationship between load and crack velocity and hence enable more accurate lifetime predictions.

TABLE V Comparison of coefficients in the Weibull exponents for reduced Weibull functions at 700° C

S (MPa)	S_{0_2}/S_{0_1}	$\left(\frac{m_2+1}{A_2}\right)^{1/m_2} \Big/ \left(\frac{m_1+1}{A_1}\right)^{1/m_1}$
~1	1.32	1.38
~100	1.31	1.52

7. Summary

STP diagrams have been established for a commercial ceramic cutting-tool material, at temperatures ranging from ambient to 1100° C. Two mechanisms have been found to be active. In air the stress corrosion mechanism, on which the STP concept is based, is dominant even at 1100° C. In a vacuum at high temperatures an energy-dissipating mechanism has been found to be active. The interaction of the two mechanisms is responsible for the subcritical crack growth at the higher temperatures. These STP design diagrams enable lifetime predictions to be made at operating temperatures for the actual component, based on tests conducted on simple geometries and loading configurations.

Another problem to be considered is the systematic influence of the experimental procedure on the statistics of the data. Such influences have to be accounted for, as has been done for the influence of loaded surface area on the strength data.

Acknowledgement

The authors gratefully acknowledge the National Science Foundation for support of this research project under Contract No. DMR-8115497.

References

1. R. W. DAVIDGE, "Mechanical Behavior of Ceramics" (Cambridge University Press, Cambridge, 1979) p. 144.
2. R. W. DAVIDGE, J. R. McLAREN and G. TAPPIN, *J. Mater. Sci.* **8** (1973) 1699.
3. K. K. SMYTH and M. B. MAGIDA, *J. Amer. Ceram. Soc.* **66** (1983) 500.
4. W. WEIBULL, *J. Appl. Mech.* **18** (1951) 293.
5. D. G. S. DAVIES, *Proc. Br. Ceram. Soc.* **22** (1973) 429.
6. W. B. HILLIG and R. J. CHARLES in "High Strength Materials", edited by V. F. Zackay (Wiley, New York, 1965) p. 682.
7. S. LAUF, PhD thesis, University of Stuttgart, West Germany (1985).
8. W. TRADINIK, K. KROMP and R. F. PABST, *Mater. Sci Eng.* **56** (1982) 39.
9. S. M. WIEDERHORN, *J. Amer. Ceram. Soc.* **50** (1967) 407.
10. A. G. EVANS and S. M. WIEDERHORN, *Int. J. Fract.* **10** (1974) 379.
11. A. BORNHAUSER, K. KROMP and R. F. PABST, in "Biomaterials 1980", edited by G. D. Winter, D. F. Gibbons and H. Blenk Jr (Wiley, New York, 1982) p. 207.
12. K. KROMP, W. TRADINIK and F. B. PRINZ, to be published.
13. R. N. STEVENS and R. DUTTON, *Mater. Sci. Eng.* **8** (1971) 220.
14. D. P. H. HASSELMAN, in Proceedings of the 15th Sagamore Army Materials Research Conference, Raquettelake, New York, August, 1968, edited by J. J. Burke, N. L. Reed and V. Weiss (Syracuse University Press, 1970) p. 297.
15. D. M. MARSH, *Proc. Phys. Soc. Lond.* **282A** (1964) 33.

16. A. G. EVANS and A. RANA, *Acta Metall.* **28** (1980) 129.
17. G. W. WEIDMANN and D. G. HOLLOWAY, *Phys. Chem. Glasses* **15** (1974) 68.
18. S. M. WIEDERHORN, in "Fracture Mechanics of Ceramics", edited by R. C. Bradt, D. P. H. Hasselman and F. F. Lange (Plenum, New York, 1978) p. 549.
19. A. BORNHAUSER, K. KROMP and R. F. PABST, *J. Mater. Sci.* **20** (1985) 2586.
20. K. KROMP, "Brittle Matrix Composites I", edited by A. M. Brandt and I. H. Marshall (Elsevier, London, 1987) 131.

Received 15 July
and accepted 22 September 1986